

Electronic Supplementary Information

Oxygen reduction reaction over $(\text{Ba},\text{Sr})_6\text{RE}_2\text{Co}_4\text{O}_{15}$ – $\text{Ba}(\text{Ce},\text{Pr},\text{Y})\text{O}_3$ composite cathodes for proton-conducting ceramic fuel cells

Toshiaki Matsui ^{a)}, *, Naoki Kunimoto ^{a)}, Kohei Manriki ^{a)}, Kazunari Miyazaki ^{a)}, Naoto Kamiuchi ^{b)}, Hiroki Muroyama ^{a)}, and Koichi Eguchi ^{a)}

- a) Department of Energy and Hydrocarbon Chemistry, Graduate School of Engineering,
Kyoto University, Nishikyo-ku, Kyoto 615-8510, Japan
- b) The Institute of Scientific and Industrial Research, Osaka University, 8-1 Mihogaoka,
Ibaraki, Osaka 567-0047, Japan

* Correspondence should be addressed to

Toshiaki Matsui
Department of Energy and Hydrocarbon Chemistry,
Graduate School of Engineering, Kyoto University,
Nishikyo-ku, Kyoto 615-8510, JAPAN
TEL: +81-75-383-7060, FAX: +81-75-383-2520
E-mail: matsui@elech.kuic.kyoto-u.ac.jp

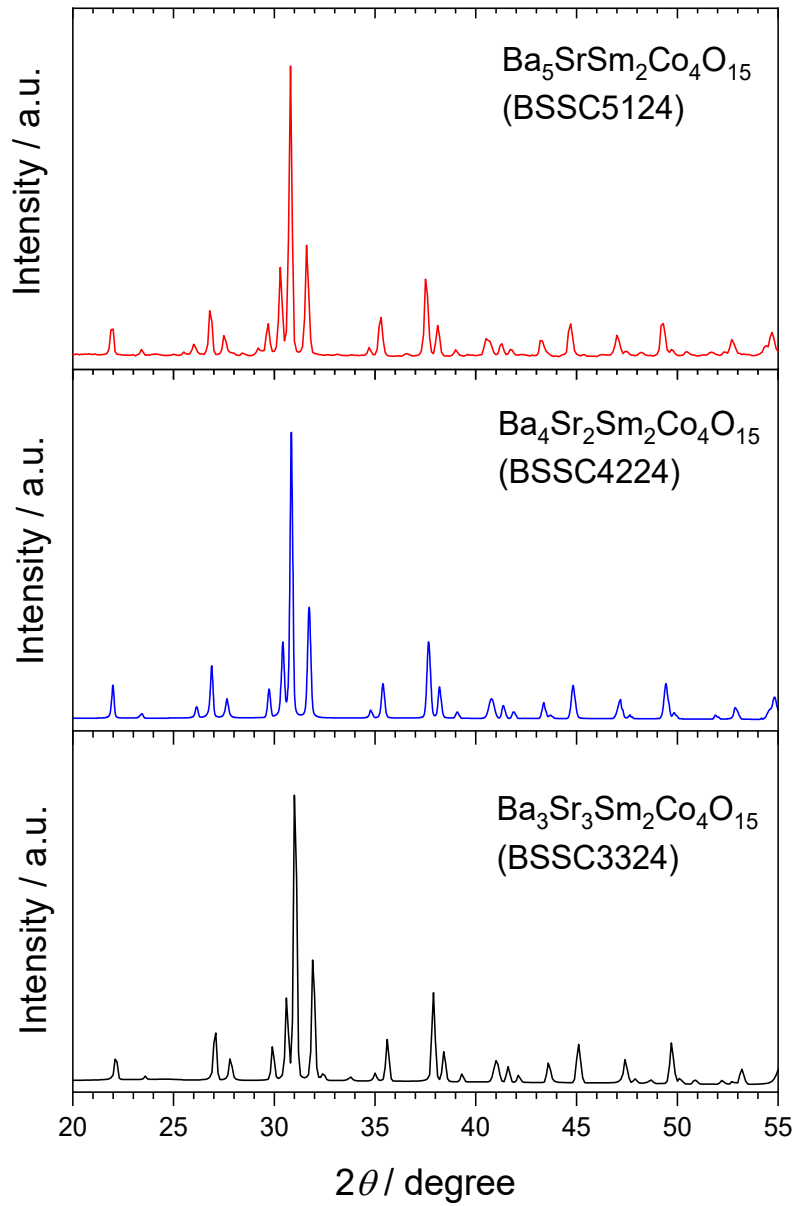


Fig. S1 XRD patterns of $(\text{Ba}_{6-x}\text{Sr}_x)\text{Sm}_2\text{Co}_4\text{O}_{15}$ ($x = 1, 2, 3$).

Fig. S1 T. Matsui et al.

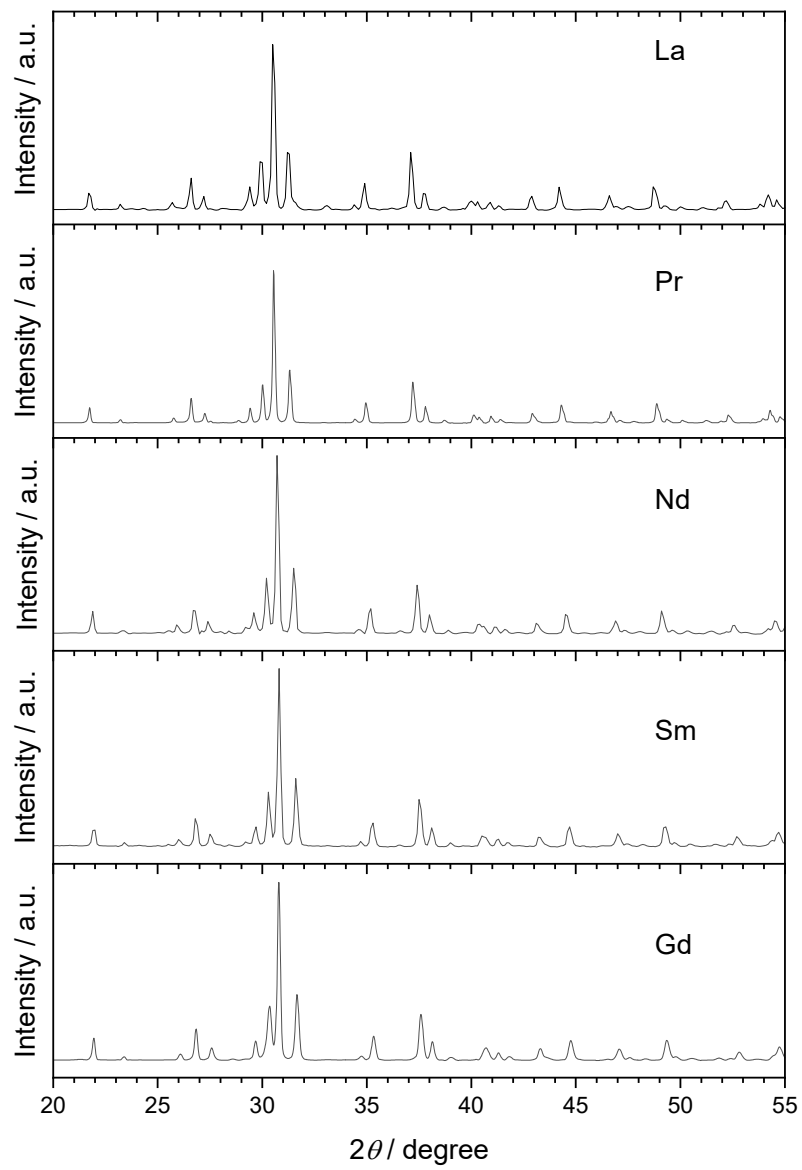


Fig. S2 XRD patterns of $\text{Ba}_5\text{Sr}RE_2\text{Co}_4\text{O}_{15}$ ($RE = \text{La}, \text{Pr}, \text{Nd}, \text{Sm}$, and Gd).

Fig. S2 T. Matsui et al.

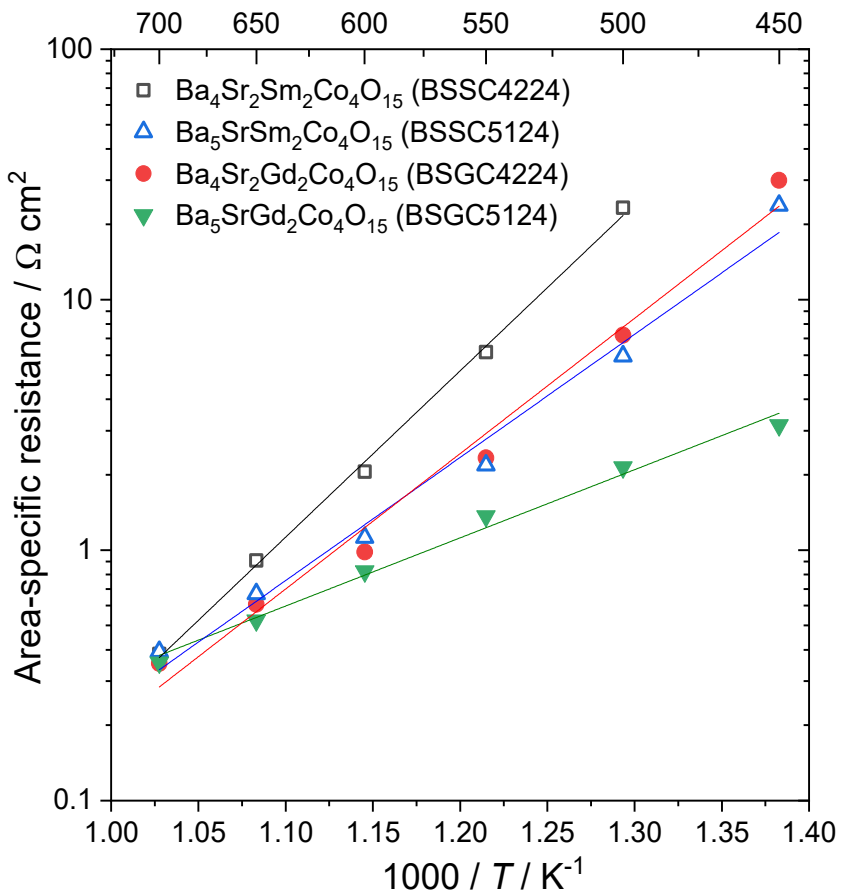


Fig. S3 Temperature dependence of area-specific resistance of $(\text{Ba}_{6-x}\text{Sr}_x)\text{Gd}_2\text{Co}_4\text{O}_{15}$ and $(\text{Ba}_{6-x}\text{Sr}_x)\text{Sm}_2\text{Co}_4\text{O}_{15}$ ($x = 1, 2$) electrodes in 3 vol.% humidified synthetic air. All oxides were fired on the BCY disk at 1200 °C.

Fig. S3 T. Matsui et al.

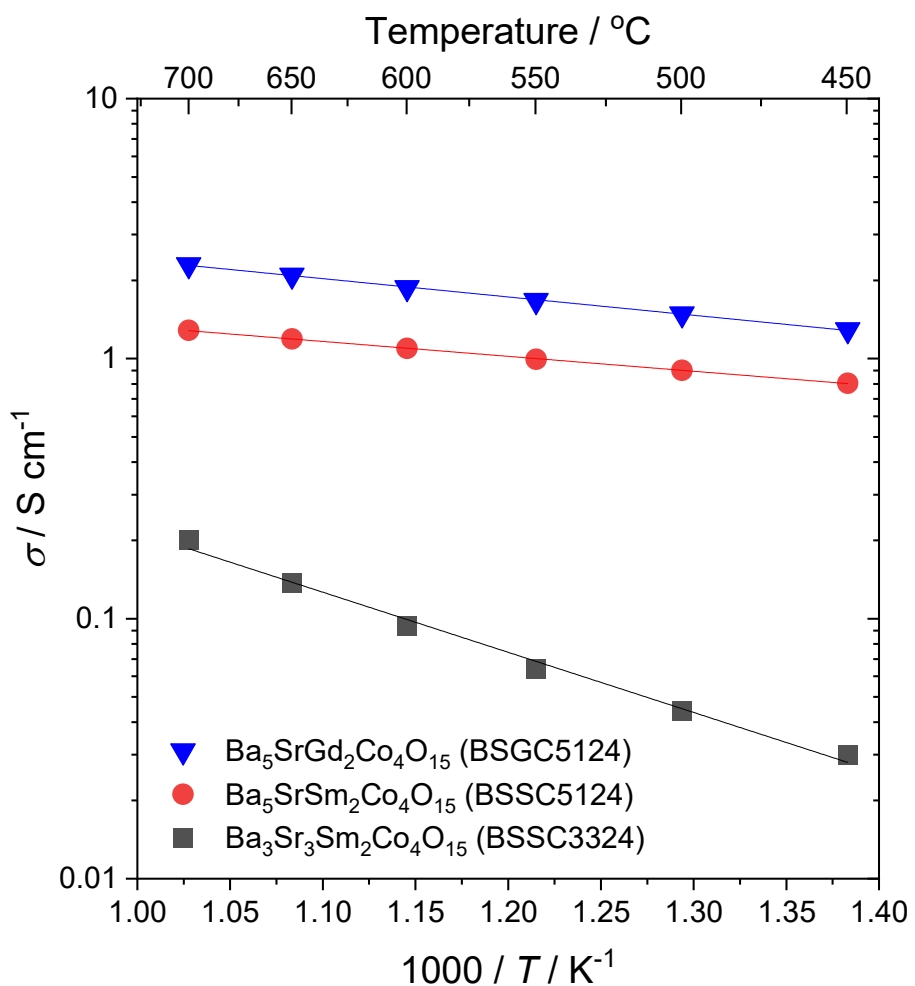


Fig. S4 Temperature dependence of total electrical conductivity of $(\text{Ba}_{6-x}\text{Sr}_x)\text{Sm}_2\text{Co}_4\text{O}_{15}$ ($x = 1, 3$) and $\text{Ba}_5\text{SrGd}_2\text{Co}_4\text{O}_{15}$ in 3 vol.% humidified synthetic air. The four-probe dc technique was applied to measure the conductivity with Ag electrodes. All oxides were sintered at 1300 °C for 5 h to prepare dense samples.

Fig. S4 T. Matsui et al.

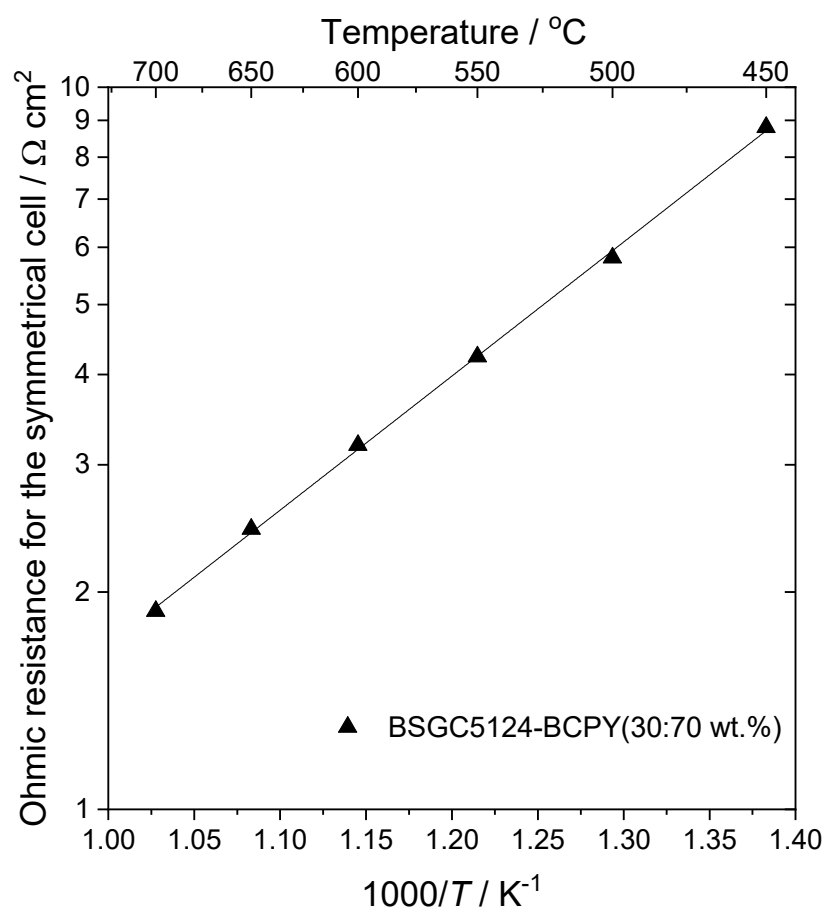


Fig. S5 Temperature dependence of ohmic resistance for the symmetrical cell employing BSGC5124-BCPY (30:70 wt.%) composite electrodes used in Fig. 4. Atmosphere; 3 vol.% humidified synthetic air.

Fig. S5 T. Matsui et al.

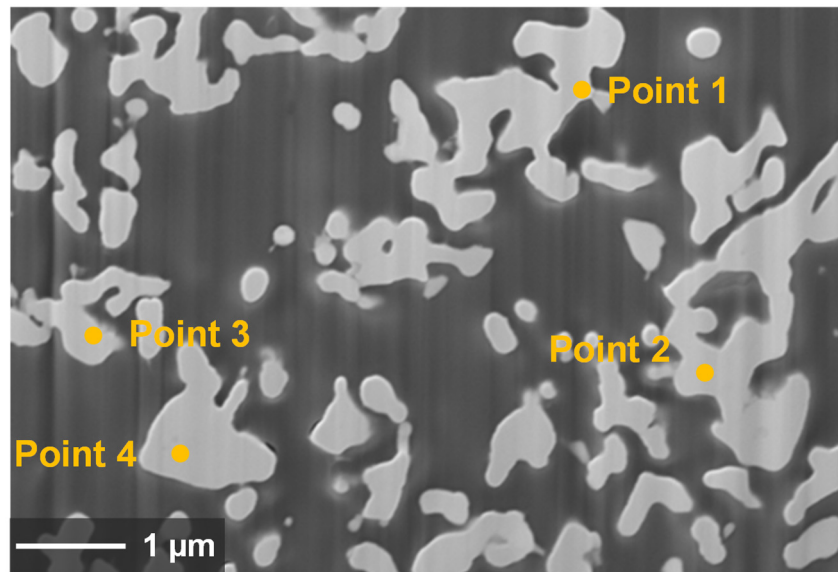


Fig. S6 Cross-sectional SEM image of the BSGC5124–BCPY (30:70 wt.%) composite electrode. The black part corresponds to the pore. Firing temperature of the composite electrode; 1000 °C.

Fig. S6 T. Matsui et al.

Table S1 Molar percent of constituent elements and phase information at each point in Fig. S6.

Point	Element / mol%								Main Phase
	Sr	Gd	Co	Ce	Pr	Y	Ba	O	
1	0.9	1.8	3.0	7.0	4.1	3.1	17.9	62.3	BSGC5124, BCPY
2	0.4	1.0	2.6	9.0	5.1	3.5	21.3	57.2	
3	0.1	0.3	1.2	10.1	4.9	3.8	20.1	59.5	BCPY
4	0.2	0.5	1.5	11.1	5.7	4.1	23.5	53.5	

Table S1 T. Matsui et al.